

Journal of Nuclear Science and Technology

ISSN: 0022-3131 (Print) 1881-1248 (Online) Journal homepage: https://www.tandfonline.com/loi/tnst20

A small long-cycle PWR core design concept using fully ceramic micro-encapsulated (FCM) and UO_2–ThO_2 fuels for burning of TRU

Gonghoon Bae & Ser Gi Hong

To cite this article: Gonghoon Bae & Ser Gi Hong (2015) A small long-cycle PWR core design concept using fully ceramic micro-encapsulated (FCM) and UO_2–ThO_2 fuels for burning of TRU, Journal of Nuclear Science and Technology, 52:12, 1540-1551, DOI: 10.1080/00223131.2015.1018364

To link to this article: https://doi.org/10.1080/00223131.2015.1018364

Published online: 11 Mar 2015.

Submit your article to this journal

Article views: 536

View related articles

View Crossmark data

Citing articles: 2 View citing articles

Full Terms & Conditions of access and use can be found at
https://www.tandfonline.com/action/journalInformation?journalCode=tnst20

Journal of Nuclear Science and Technology, 2015
Vol. 52, No. 12, 1540–1551, http://dx.doi.org/10.1080/00223131.2015.1018364

Taylor & Francis
Taylor & Francis Group

ARTICLE

A small long-cycle PWR core design concept using fully ceramic micro-encapsulated (FCM) and UO_2–ThO_2 fuels for burning of TRU

Gonghoon Bae* and Ser Gi Hong

Department of Nuclear Engineering, Kyung Hee University, Deogyeong-daero, GiHeung-gu, Yongin, Gyeonggi-do 446-701, Korea

(*Received 17 December 2014; accepted final version for publication 7 February 2015*)

In this paper, a new small pressurized water reactor (PWR) core design concept using fully ceramic micro-encapsulated (FCM) particle fuels and UO_2–ThO_2 fuels was studied for effective burning of transuranics from a view point of core neutronics. The core of this concept rate is 100 MWe. The core designs use the current PWR-proven technologies except for a mixed use of the FCM and UO_2–ThO_2 fuel pins of low-enriched uranium. The significant burning of TRU is achieved with tri-isotropic particle fuels of FCM fuel pins, and the ThO_2–UO_2 fuel pins are employed to achieve long-cycle length of ~4 EFPYs (effective full-power year). Also, the effects of several candidate materials for reflector are analyzed in terms of core neutronics because the small core size leads to high sensitivity of reflector material on the cycle length. The final cores having 10 w/o SS303 and 90 w/o graphite reflector are shown to have high TRU burning rates of 33%–35% in FCM pins and significant net burning rates of 24%–25% in the total core with negative reactivity coefficients, low power peaking factors, and sufficient shutdown margins of control rods.

Keywords: TRU burning; small long-cycle PWR; FCM particle fuel

1. Introduction

One of the obstacles for the sustainable deployment of nuclear energy is the accumulation of spent fuels from commercial pressurized water reactors (PWRs) and the difficulties in their management. In particular, of the nuclides contained in PWR spent fuel, TRU (transuranics) nuclides are the main contributors to the long-term radiotoxicities and heat generation in spite of their small contents in PWR spent fuel [1]. In principle, the fast reactors using metallic coolants such as sodium and lead-alloys can provide an ideal nuclear park coupled with PWR for transmutation or incineration of TRUs combined with a closed fuel cycle (i.e., recycling of almost all actinides) [2–4]. The high TRU burning capability of fast reactors is contributed from higher fission-to-capture reaction ratio and larger number of excess neutrons per fission than thermal spectrum reactors [2]. However, the fast reactor cores have not been fully commercialized due to their technological and political issues, and they have been classified as the future generation IV reactors. In particular, the full utilization of fast reactors for TRU burning requires recycling of almost all actinides to reduce the amount of actinides going into the waste stream, and the spent fuels from fast reactors are discharged with high discharge burnup, which requires reprocessing of them with remote processing tools in the shielded facilities, and these facts can be involved with political issues such as nuclear proliferation. In addition, thermal spectrum reactors including PWRs have much smaller values of fission-to-capture ratio than fast reactors and so it has been known that the number of recycling is typically limited up to less than five or four times due to degradation of plutonium quality and accumulation of minor actinides that are main contributors to heat generation and to the resulted degradation of safety-related parameters such as void coefficient [5,6]. One of the advantages of thermal spectrum reactors for TRU burning is much larger fission cross sections than in the fast spectrum reactors. Recently, there have been several research works on the deep burning of PWR spent fuel TRUs in commercial PWRs [7,8], where the deep burning of TRUs with a single pass (i.e., not recycling) was achieved using fully ceramic micro-encapsulated (FCM) fuels due to their superior high burnup performance [9,10]. In the FCM pins, TRISO (tri-Isotropic) particle fuels comprising TRU containing central kernel and its surrounding buffer layers are distributed in SiC matrix which has high thermal conductivity [10]. Due

*Corresponding author. E-mail: sergihong@khu.ac.kr

© 2015 Atomic Energy Society of Japan. All rights reserved.

to these features, the FCM fuel has been shown to have extraordinary fission product retention and low fuel temperature due to its high thermal conductivity, and therefore, the FCM fuel has been considered as an accident tolerant fuel. Although the previous studies in commercial-scale PWR [7,8] showed high burning rate of TRU in FCM fuel, the net destruction or burning rate of TRU over the core was almost zero due to the generation of TRUs in UO_2 pins. In this work, the cores are designed to have significant net TRU destruction rates by changing the fuel assembly and FCM fuel designs.

In this paper, small-size cores of 100 MWe rather than large-scale commercial ones are considered to reduce the burden of reprocessing for initial FCM fuel fabrication and of the initial investment. The cores use single-batch refueling scheme, and therefore, all fuel assemblies are discharged at the end of every cycle. ThO_2–UO_2 fuel pins, where uranium enrichment is less than 20 wt%, are introduced instead of UO_2 pins to improve net destruction of TRUs over the core and to achieve the long cycle length of ~4 EFPYs. Therefore, the fuel assemblies used in this study consist of ThO_2–UO_2 pins and FCM fuel pins. One of the important parts done in this work is on a study of the reflector effect on the core performances. For this purpose, several reflector materials such as SS303, graphite, lead, and beryllium are considered to enlarge long cycle length because the neutronic performance of reflectors can give significant effect on the cycle length of small cores, and several different types of burnable absorbers are considered to reduce initial excess reactivity and control the power peaking. For burnable absorbers, the Gd_2O_3 *BISO* (bi-Isotropic) particles used in the previous studies [7,8] are considered in FCM pins. Additionally, to further reduce the excess reactivity, ZrB_2 coating as in *integral fuel burnable absorber* (IFBA) is considered in some of ThO_2–UO_2 fuel pins, and B_4C BISO particles are newly considered in FCM fuel pins. Two final candidate cores having solid reflector of 10 w/o SS303 and 90 w/o graphite are designed and their detailed neutronic analyses are performed to show their feasibility, but the safety analysis has not been performed yet.

The first core has relative more complicated loading pattern and higher critical boron concentration (CBC), but it has longer cycle length and high net destruction rate of TRU over core. This core was used to analyze the effects of the reflectors on the core performances. The second core was designed to have simple two-region fuel loading pattern and to reduce CBC. This second core has a shorter cycle length, a smaller net destruction rate of TRU over core but much smaller CBC than the first one.

This paper is organized as follows. Chapter 2 provides computational procedure including codes and Chapter 3 describes the fuel assembly design concepts and their neutronic performances. The core designs are also described and then their performances are analyzed in Chapter 3. The conclusions including summaries are given in Chapter 4.

2. Computational procedure and codes

The typical two-step procedure used in designing the conventional PWR cores is used in our study. However,the difficulty occurs in the treatment of the self-shielding effect resulting from the use of TRISO fuel and BISO burnable absorber particles in FCM pins, which leads to complicated double heterogeneities. The first part of the two-step procedure consists of fuel assembly depletion and neutron transport calculations, which give the two-group homogenized fuel assembly cross sections as the function of burnup, soluble boron concentration, moderator density, fuel temperature, and so on. For this purpose, DeCART2D code [11] developed at Korea Atomic Energy Research Institute (KAERI) was used. This code uses method of characteristics (MOC) to solve multigroup transport equation and the Krylov subspace method to solve the depletion equations. Also, this code uses the subgroup method for resonance self-shielding treatment with the use of Sanchez's method to consider the double heterogeneities of randomly distributed particles containing resonance absorbers. The multigroup cross-section library for DeCART2D is the KARMA 47 group cross-section library which was generated based on ENDF/B-VII.r0. However, we newly generated the resonance integrals for three major resonance nuclides (i.e., ^{232}Th, ^{235}U, ^{238}U) by using UO_2–ThO_2 pin model [12], and then they were adjusted such that the one-group effective resonance cross sections over the resonance energy range are the same as those estimated using the McCARD code [13], which is a Monte Carlo code developed by Seoul National Laboratory. The second part of the two-step method is to analyze the core using a two-group nodal diffusion calculation code. MASTER [14] developed at KAERI was used for this purpose. This code employs several different advanced nodal methods and provides various capabilities including static and transient calculations coupled with thermal-hydraulics calculations. In particular, in this work, the homogenized reflector cross sections for core calculations were accurately generated using two-dimensional (2D) whole core heterogeneous transport calculation with DeCART2D in order to accurately consider large leakage effects through the small cores.

3. Design and analyses of fuel assemblies and cores

3.1. *Fuel assembly designs and analyses*

The reference fuel assembly used in this work [12,15] is the ABB/CE 16 × 16 type which has four large water holes for control rods and one central large water hole for in-core instrumentation. As mentioned in Section 1, the TRUs to be transmuted are contained in the central kernel of TRISO particles in FCM fuel pins. The

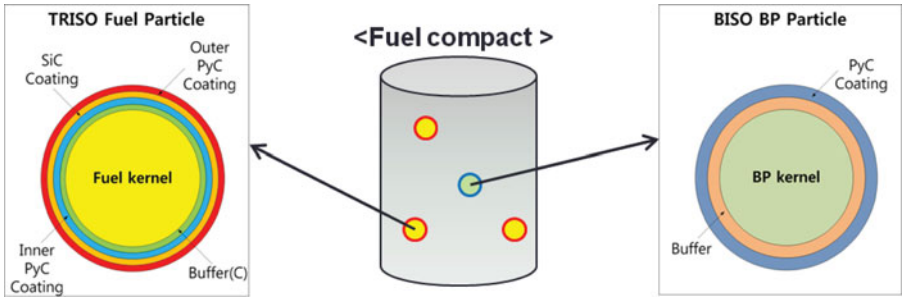


Figure 1. Description of FCM fuel and TRISO/BISO particles.

FCM fuel pins use the identical fuel cladding tubes of the ABB/CE 16 × 1 6 type fuel assembly. The TRU composition is from PWR spent fuel with 50 MWD/kg burnup and 10 years cooling time. Actual composition of TRISO kernel is 24.3 v/o SiC and 75.7 v/o TRU-O_2, and its density is assumed to be 9.46 g/cm^3. A TRISO particle fuel consists of a central kernel and the surrounding four outer buffer layers (i.e., 100 μm thick buffer layer, 35 μm thick inner PyC layer, 35 μm SiC layer, and 40 μm thick outer PyC layer) providing an effective pressure-tight enclosure. Because of these features, the FCM fuel is characterized by its high thermal conductivity and excellent irradiation performance likely to be achievable in PWRs, and the chemically stable properties of SiC combined with these features are considered to make the FCM-spent fuel an excellent long-term waste disposal material. Also, BISO particles having burnable absorbing material in their central kernels are employed to reduce the excess reactivity and to control power peaking. These particles with different packing fractions from the TRISO particles are also distributed in the SiC matrix of FCM fuel pins. **Figure 1** shows an FCM fuel pin, TRISO particle fuels, and BISO burnable absorber particles. The kernel diameters and packing fractions of TRISO and BISO particles are used as the design parameters. Gd_2O_3, Er_2O_3, and B_4C are considered as the kernel materials for burnable absorber in BISO particle [16]. The BISO kernel is surrounded by 18 μm thick buffer and 23 μm thick PyC layers. In our new fuel assemblies, UO_2–ThO_2 fuel is employed to replace the conventional UO_2 fuel to achieve long cycle length and net destruction rate of TRU, and ThO_2 is also contributed to reducing excess reactivity [17,18]. Also, to further reduce the excess reactivity, IFBA-like concept using ZrB_2 coating on the UO_2–ThO_2 pins is considered. The boron enrichment in ZrB_2 is 35% B-10 and the coating thickness is 0.002 cm.

Before going to the detailed fuel assembly design, the effect of ThO_2 combined with uranium enrichment on the neutronic characteristics such as cycle length and moderator temperature coefficient (MTC) is analyzed to determine the weight fraction of ThO_2 in UO_2–ThO_2. For this purpose, a reference fuel assembly is selected and one-fourth of the reference fuel assembly is shown in **Figure 2**. As shown in Figure 2, the reference fuel assembly consists of 124 FCM pins and 112 UO_2–ThO_2 pins.

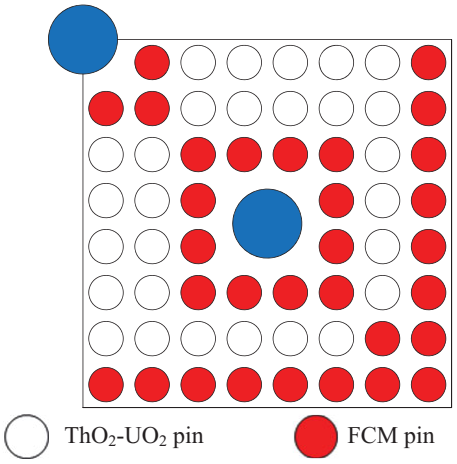


Figure 2. Configuration of the reference fuel assembly.

For this case, the kernel diameters of TRISO and BISO particles are 600 and 500 μm, respectively. Also, the burnable absorber material is Gd_2O_3 in BISO particles.

For this reference assembly configuration, two different initial k_{inf} values of 1.095 and 1.233 are considered, and the uranium enrichments of UO_2 are searched such that the assembly has the specified initial k_{inf} values. For the low initial k_{eff} case, the packing fractions of TRISO and BISO particles are 42.5% and 2%, respectively, while they are 47% and 0.5% for the high initial k_{inf} case. A soluble boron concentration of 500 ppm is considered in the fuel assembly calculations. **Figures 3** and **4** compare the evolutions of k_{inf} over 1850 EFPDs for the low and high initial k_{inf} cases, respectively. For each of the initial k_{inf} cases, the four different ThO_2 contents of 0 wt% (i.e., no thorium case), 25, 35, 50, and 75 wt% are considered to show the effect of ThO_2 weight fraction, while uranium enrichment is adjusted to have the same initial k_{inf} for all the ThO_2 cases.

These figures show that a larger content of ThO_2 with a fixed initial k_{inf} leads to a longer cycle length but a higher ThO_2 content than 50 wt% gives only small effects on the cycle length. This means that ThO_2 enlarges the cycle length with a fixed initial excess reactivity. Also, the variations of MTCs are compared in **Figure 5** for the high initial k_{inf} case. In Figure 5, it is noted that MTCs are all negative over 1900 EFPDs and that the

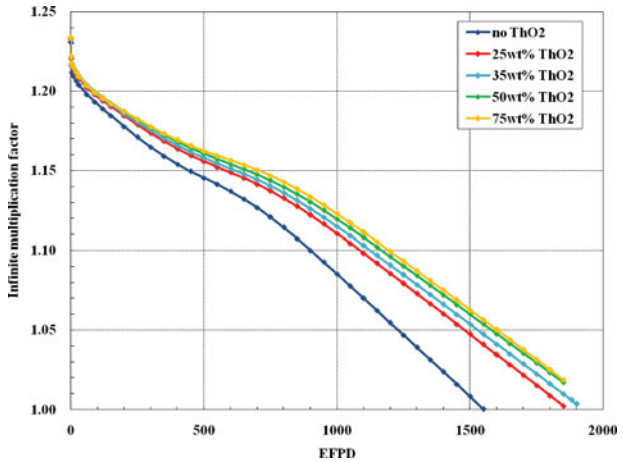


Figure 3. Comparison of the changes of the infinite multiplication factors for the high initial k_{inf} case.

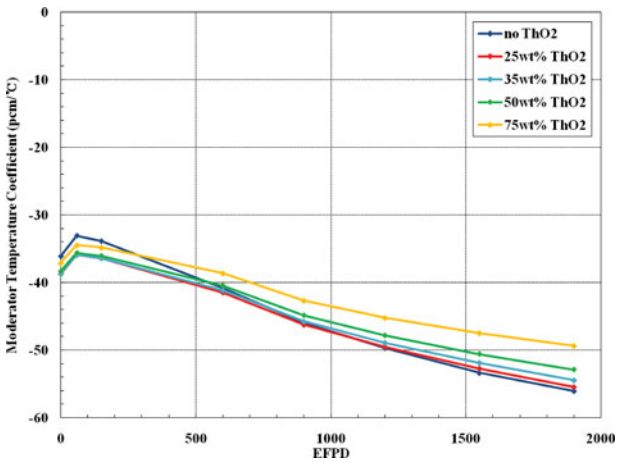


Figure 5. Comparison of the changes of MTCs for the high initial k_{inf} case.

no-thorium case has the least negative MTC at fresh state, while higher ThO_2 content cases have less negative MTCs than the lower ThO_2 content cases as fuels deplete. As will be shown in Section 3.2, the cores designed in this work have strong negative MTCs at end of cycle (EOC) under hot full-power condition but too negative MTCs can be problematic under the accidents related with cold water inflow. Therefore, the above analysis shows the addition of ThO_2 which helps the core to have less negative MTC at EOC. **Table 1** summarizes the initial uranium enrichments and the amount of TRUs generated in UO_2–ThO_2 pins versus ThO_2 weight fraction both for the high and low initial k_{inf} cases. As expected, Table 1 shows that the initial uranium enrichment increases and the amount of TRUs in UO_2–ThO_2 pins decreases as ThO_2 weight fraction. For the high initial k_{inf} case, 50 wt% ThO_2 leads to the initial uranium enrichment of 17.0 wt% and the amount of TRU generation in UO_2–ThO_2 pins is reduced by ~38% in comparison with the case having no thorium. From this sensitivity study on ThO_2 content, 50 wt% of ThO_2 is selected as a reference ThO_2 content to satisfy the uranium enrichment limit and to have long cycle length under a fixed initial reactivity.

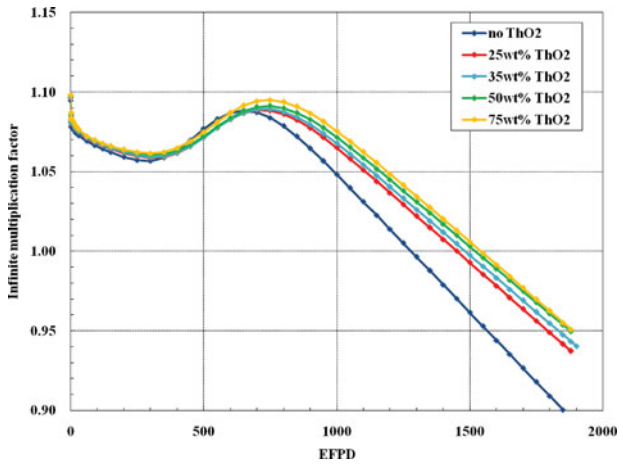


Figure 4. Comparison of the changes of infinite multiplication factors for the low initial k_{inf} case.

Next, five fuel assemblies are designed such that the cores have long cycle length of ~4.0 EPFYs and a significant TRU burning rate. Also, the burnable absorbers of advanced concept such as BISO particles in FCM fuel and IFBA-like coating of ZrB_2 in UO_2–ThO_2 fuel are also employed to reduce excess reactivity and to control power peakings.**Table 2** summarizes the design parameters such as TRISO and BISO packing fractions and kernel diameters for these five fuel assemblies.

Figure 6 shows the configurations for the four fuel assemblies which will be used in the core design A described in Section 3.2. The fuel assemblies of types A and B use the configuration shown in Figure 6(a), while the ones of types C and D use the configuration shown in Figure 6(b). These four fuel assemblies use BISO burnable absorber particles, but UO_2–ThO_2 fuels do not have burnable absorbers, and the ThO_2 content is 50 wt% in UO_2–ThO_2 fuel. In the fuel assemblies of types A and B, the enrichment splittings are employed to reduce pin power peaking by locating the low uranium enrichment UO_2–ThO_2 pins near the water holes and BISO particles of Gd_2O_3 kernel are used in FCM fuel pins. For the type A, the uranium enrichments are 11 and 8.5 wt% for low and high uranium enrichment pins, respectively. The fuel assembly of type B has slightly higher TRISO and lower BISO packing fractions, and higher uranium enrichments than those of the fuel assembly of type A. On the other hand, the fuel assemblies of types C and D do not use uranium enrichment splitting and they use higher uranium enrichments than the previous two fuel assemblies. The fuel assembly of type C uses two different BISO particles of Gd_2O_3 and Er_2O_3 kernels to mitigate the reactivity rising after depletion of Gd_2O_3 which was observed in the fuel assemblies of types A and B [16].

The configuration of the fuel assembly of type E which is used in the Core Design B is shown in **Figure 7**

Table 1. Comparison of initial uranium enrichments and TRU generations in UO_2–ThO_2 pins versus ThO_2 weight percent.

		ThO_2 weight fraction				
Initial k_{inf}	Initial TRU mass	No ThO_2	25 wt% ThO_2	35 wt% ThO_2	50 wt% ThO_2	75 wt% ThO_2
1.095	Initial uranium enrichment (wt%)	3.90	7.20	8.80	12.20	25.30
	[a]TRU generation in UO_2–ThO_2 pins (kg)	1.59	1.33	1.21	1.02	0.64
1.233	Initial uranium enrichment (wt%)	5.05	9.99	12.30	17.00	34.40
	[a]TRU generation in UO_2–ThO_2 pins (kg)	1.60	1.33	1.20	1.00	0.62

Note: [a]210cm fuel height is assumed and evaluated at 1700EFPD.

and the design parameters for this are also summarized in Table 2. Actually, this fuel assembly was designed to further reduce the CBC (i.e., excess reactivity) of Core Design A. As shown in Figure 7, this fuel assembly has a reduced number of FCM fuel pins than the fuel assemblies described above, and the FCM pins are scattered over the fuel assembly while the FCM pins are located along lines in the fuel assemblies of type A, B, C, and D. The kernel diameters of TRISO particles are decreased from 600 to 500 μm in this fuel assembly, but a 0.002 cm thick ZrB_2 coating of 35% B-10 is employed in 28 UO_2–ThO_2 fuel pins. To further reduce the initial reactivity, BISO particles having B_4C (natural boron) kernels were employed in all the FCM fuel pins. The ThO_2 content for this new fuel assembly is increased to 60 wt% in order to mitigate the reduction of net TRU destruction rate due to the reduction of the number of the FCM fuel pins. The uranium enrichments of this new fuel assembly are 13.5 wt%.

The evolutions of the infinite multiplication factors (k_{inf}) over time for these five fuel assemblies described above are compared in **Figure 8** and those of the pin power peaking factors are compared in **Figure 9**. In Figure 8, it is noted that the fuel assembly of type E shows different shape of k_{inf} evolution due to the use of IFBA-like concept of burnable absorber in comparison with the fuel assemblies of types A, B, C, and D. Figure 9 shows that the pin power peaking factors increase as time in the fuel assembly of type E and this change trend is different from those of the fuel assemblies of types A, B, C, and D, where pin power peaking factors decrease and then increase as time because the initial maximum power peaking occurs in FCM pins and then moves into UO_2–ThO_2 pins after depletion of TRU. Also, all the fuel rods having burnable absorber materials considered in this work are designed to have 21.5 cm thick cutback regions in the ends of top and bottom where the burnable absorber materials (i.e., BISO particles or ZrB_2) are not used in order to reduce the axial power peaking.

3.2. *Small PWR core design and performance analysis*

3.2.1. *Analysis of the effects of reflector materials*

In this section, small PWR cores are designed by using the new fuel assemblies described in Section 3.1. For the reference core, 308 MWt power rating is considered and a low average linear power density of 120 W/cm is adopted to achieve long cycle length and large thermal margin. The conventional water reflector is used for the reference core. As mentioned in Section 1, the core uses

Table 2. Design parameters for five fuel assemblies used in Core Designs A and B.

Type	A	B	C	D	E
			FCM pin		
Kernel diameter (μm)	600	600	600	600	500
Matrix	SiC	SiC	SiC	SiC	SiC
Packing fraction (%, TRISO/BISO)	44/4.0	45/3.5	47/1.5 + 1.5	48/1.0	45/2.0
Burnable absorber material	Gd_2O_3	Gd_2O_3	$Gd2O_3$, Er_2O_3	Gd_2O_3	B_4C
			ThO_2–UO_2 pin		
Uranium enrichments	[a]11%/[b]8.5%	[a]12.5%/[b]10%	16.0%	17.0%	13.5%
ThO_2 weight percent	50.0 wt%	50.0 wt%	50.0%	50.0%	60.0%
IFBA-like concept					
ZrB_2 coating thickness	N/A	N/A	N/A	N/A	0.002cm
B-10 enrichment	N/A	N/A	N/A	N/A	35.0 wt%

Notes: [a]High enrichment UO_2–ThO_2 pins and [b]low enrichment UO_2–ThO_2 pins

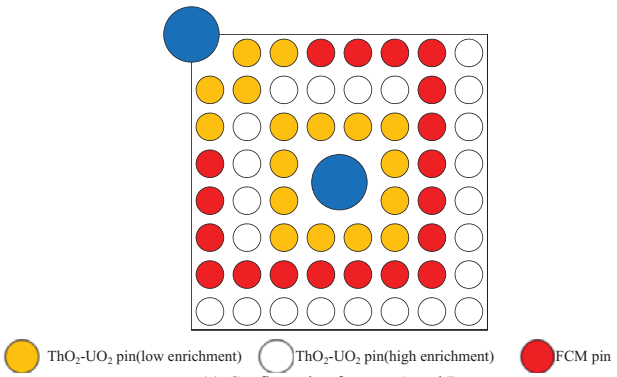


Figure 6. Configurations of the fuel assemblies used in Core Design A.

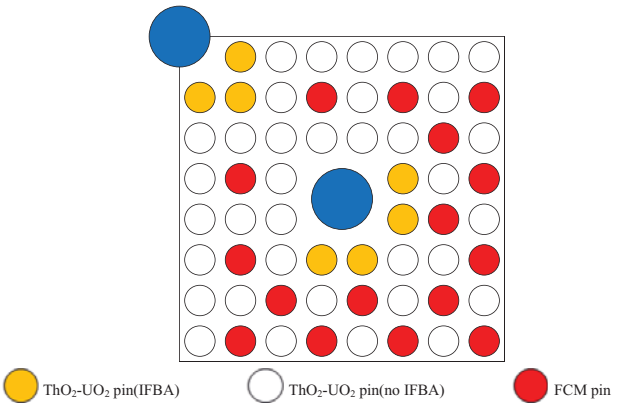


Figure 7. Configurations of the fuel assembly type E.

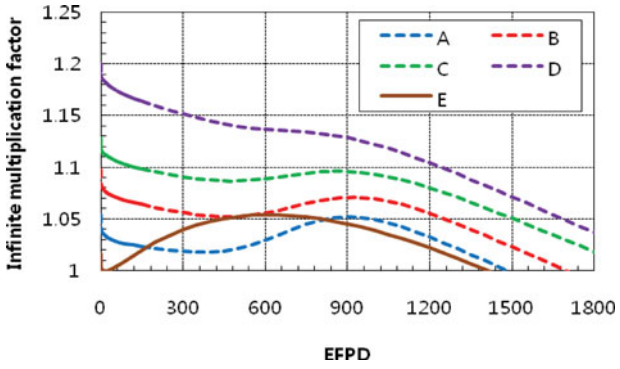


Figure 8. Comparison of the changes of the infinite multiplication factors for the designed fuel assemblies.

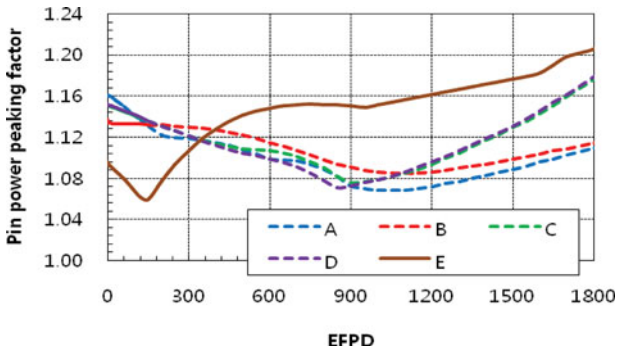


Figure 9. Comparison of changes of the pin power peaking factors for the designed fuel assemblies.

a single batch fuel management scheme without recycling. The active core height is 210 cm. **Figure 10** shows the loading pattern of the reference core [19]. As shown in Figure 10, the core consists of four different types of fuel assemblies (i.e., A, B, C, and D types described in Section 3.1) that are surrounded by the water reflectors. The loading pattern is a simple out-in type where high-reactive fuel assemblies are loaded in the outer region while low-reactive ones in the inner region for power flattening. The total number of fuel assemblies is 57. In Figure 10, the reflectors are denoted by R2 and R3. For this loading pattern, we also considered different reflector materials to show the effect of reflector materials on the core neutronic performances including cycle length [19].

The considered reflector materials include graphite, SS303, lead, and metallic beryllium. Although realistic fabrications of the reflectors using pure graphite, pure lead, and pure beryllium may be not practical, it is assumed that the combinations of these pure materials and structural material such as SS303 are possible and the

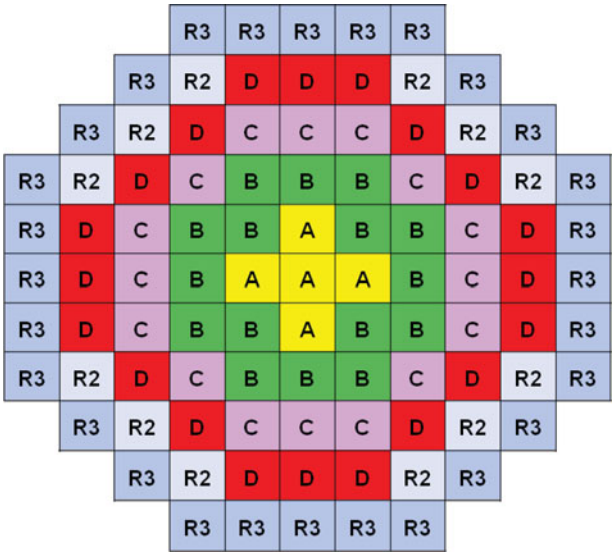


Figure 10. Core loading pattern including reflector assemblies for Core Design A.

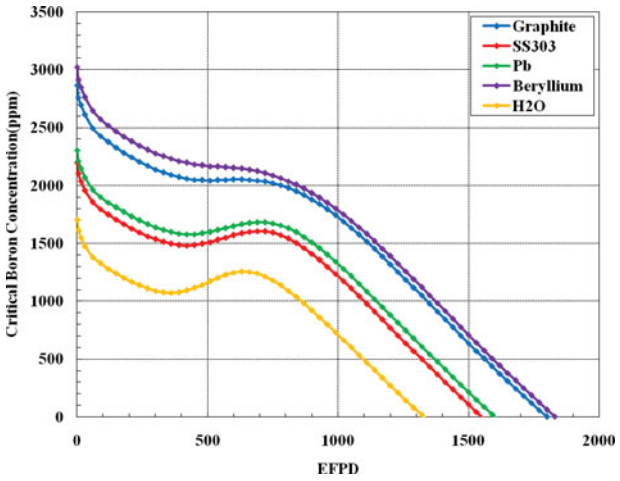


Figure 11. Comparison of critical boron concentrations for the cores having different reflector.

cores using the combinations of these pure materials and SS303 give the performances that are in the range of the results given in this work. **Figure 11** compares the evolutions of the critical boron concentration (CBC) for the cores having different reflectors.

It is shown from Figure 11 that all the cases have much longer cycle length than the reference core having water reflector and that beryllium is the most effective reflector in terms of cycle length. The graphite and beryllium reflector cores are shown to have much longer cycle length (∼1800 EFPD) by ∼500 EFPD than the reference core having water reflector. The reference core has ∼1300 EFPD cycle (i.e., ∼3.5 EFPY) length, and the cores having lead and SS303 reflectors have 1600 EFPD (i.e., ∼4.4 EFPY) and 1500 EFPD (i.e., ∼4.1 EFPY), respectively. However, it should be noted that the cores having solid reflector have high initial CBC in comparison with the reference core having water reflector. The 3D power peaking factors (denoted by F_{xyzp} or F_q) over time are compared in **Figure 12**. From this figure, it

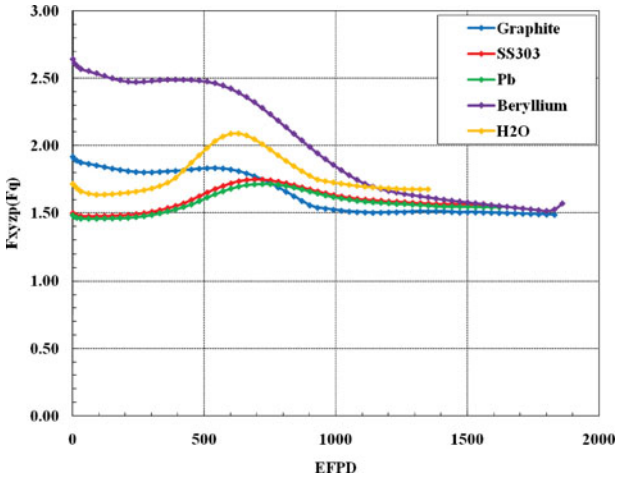


Figure 12. Comparison of 3D power peaking factors for the cores having different reflector.

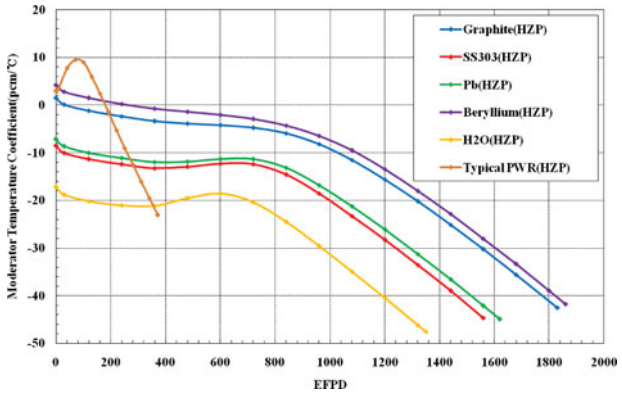


Figure 13. Comparison of MTCs (at hot zero power) for the cores having different reflector.

is noted that the beryllium reflector causes high power peaking in the fuel assemblies adjacent to the reflectors due to its higher moderating power. On the other hand, all the other cores have reasonable level of 3D power peaking factors lower than 2.2 because the typical design limit on 3D power peaking factor is 2.5–2.7. In this work, the upper limit of 3D power peaking factor is set to 2.5. In particular, the cores having SS303, graphite, and lead reflectors have very low 3D power peaking factors lower than 2.0. The radial power peaking factors (F_r) are also analyzed but not given here for simplicity. Our design upper limit of the radial power peaking factor is 1.65 and the results showed that all the cores except for the beryllium reflector core also has their radial power peaking factors than the upper limit.

Next, the MTC is analyzed for the cores having different reflectors. **Figures 13** and **14** compare moderator temperature coefficients in hot zero power (HZP) and hot full power (HFP), respectively. In these figures, the MTC values for the YongGwang unit 3 cycle 1 were also given to show the differences between the commercial PWR and the new small PWR cores considered in this work. For all the cores shown in Figures 13 and 14, MTC values show smaller changes in magnitude through the first half of cycle in comparison with the YongGwang

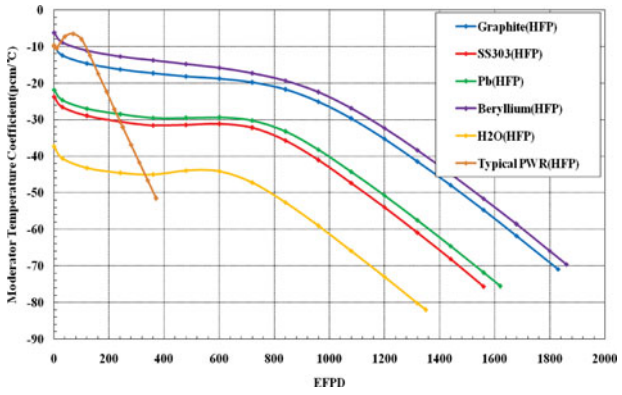


Figure 14. Comparison of MTCs (at hot full power) for the cores having different reflector.

Table 3. Comparison of TRU mass inventories (kg) for the cores having different reflectors.

Reflector material	Water	Graphite	SS303	Lead	Beryllium
TRU mass in BOC			653.6		
TRU mass in EOC	531.5	473.5	506.1	516.2	470.0
[a]Net TRU destruction rate(%) in a core	18.8	27.6	22.6	21.1	28.2
[a]TRU destruction rate(%) in FCM pins	27.1	37.9	31.9	33.1	38.6

Note: [a]Destruction rate = (mass at BOC − mass at EOC)/mass at BOC × 100.

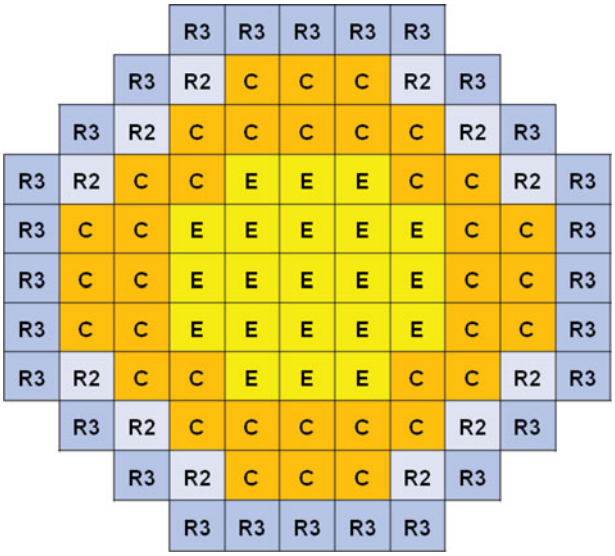


Figure 15. Core loading pattern including reflector assemblies for Core Design B.

unit 3 cycle 1, and after this period, MTC values rapidly become more negative. For the HZP case, in spite of their high CBC values, new small PWR cores have negative MTC values over their cycles except for slightly positive values near the beginning of the cycle only for the cores having beryllium and graphite reflectors, but these slightly positive MTCs are less positive than those of the YongGwang unit 3 cycle 1. From these figures, it is shown that the reference core having water reflector has the largest negative MTC values. Also, it is clear that the change trend of MTCs over time is similar to the change of CBCs. For the HFP case, all the new small PWR cores also show negative MTC values over their cycle lengths and it is noted that the new cores have very high negative MTC but too high negative MTC may lead to an insertion of large positive reactivity under accidents related with cold water inflow such as main steam line break. However, the safety analyses have not been performed in this work because it is out of the scope of this work.

Table 3 compares the TRU mass inventories and their changes from BOC to EOC. The initial TRU loading in the FCM pins of the cores is 653.6 kg, which approximately corresponds to the amount of TRU annually discharged from three units of 1000 MWe commercial PWR. Table 3 shows that the new cores give 27%–39% TRU destruction rates through FCM pins and 19%–28% net TRU destruction rates over the cores. In particular, the cores having graphite and beryllium reflectors have higher net TRU destruction rates of 27.6% and 28.2%, respectively, due to longer cycle lengths than the other cores.

3.2.2. *Comparative performances analysis of the final cores*

Based on the results of Section 3.2.1, the 10 w/o SS and 90 w/o graphite was selected as the final candidate of the reflector in order to achieve long cycle length without significantly large power peaking. This core having the loading pattern given in Figure 10 is designated as Core Design A. However, from the previous results described above, it is expected that this core will still have large initial CBC due to its large initial excess reactivity. Therefore, new core Core Design B is designed to reduce CBC by reducing the excess reactivity and to have the simpler fuel loading pattern than the Core Design A. For this purpose, we used the types C and E fuel assemblies described in Section 3.1. In the type E fuel assembly, the B_4C (natural boron) burnable poison BISO particles are used in FCM fuel pins and a 0.002 cm thick layer of ZrB_2 (35% B-10) of IFBA-like concept is used in 28 UO_2–ThO_2 fuel pins in order to further reduce the excess reactivity. The detailed descriptions for these fuel assembly types are given in Section 3.1. Also, for the Core Design B, we reduced the active fuel length from 210 to 190 cm to reduce neutron leakage by achieving H/D ratio of ∼1.0, and the thermal power is slightly reduced from 308 to 300 MWt. The loading pattern of Core Design B where higher reactive (type C) and lower reactive fuel assemblies (type E) are loaded in inner and outer regions, respectively, is shown in **Figure 15**.

Figure 16 compares the evolutions of CBCs of Core Designs A and B, while **Figure 17** the evolutions of the 3D and 2D power peaking factors. As shown in Figure 16, Core Design B has much lower CBC values, while Core Design B has shorter cycle length of ∼1440 EFPDs (i.e., ∼3.95EFPYs) than Core Design A. Figure 17 shows that Core Design B has higher power peaking factors than Core Design A, but they are still much less than their upper limits. Their 3D and 2D power peaking factors are lower than 1.8 and 1.5, respectively, over their cycles.

The MTC values at HZP and HFP are compared in **Figures 18** and **19**, respectively. Their MTC values are compared with the YongGwang unit 3 cycle 1 as

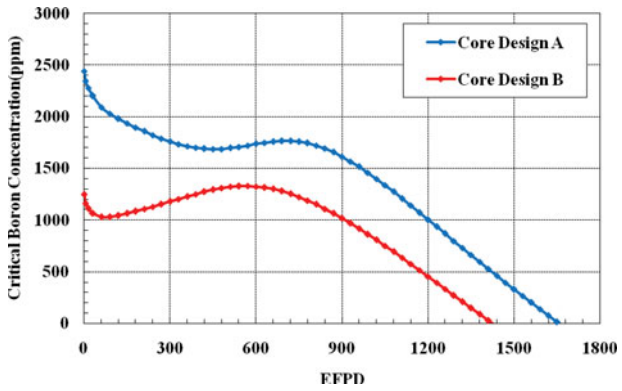


Figure 16. Comparison of critical boron concentrations for Core Designs A and B.

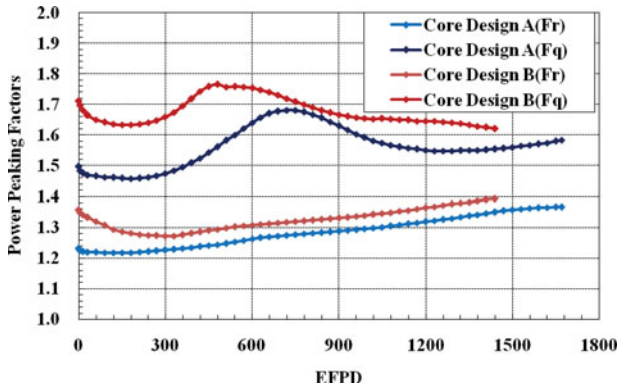


Figure 17. Comparison of 2D and 3D power peaking factors for Core Designs A and B.

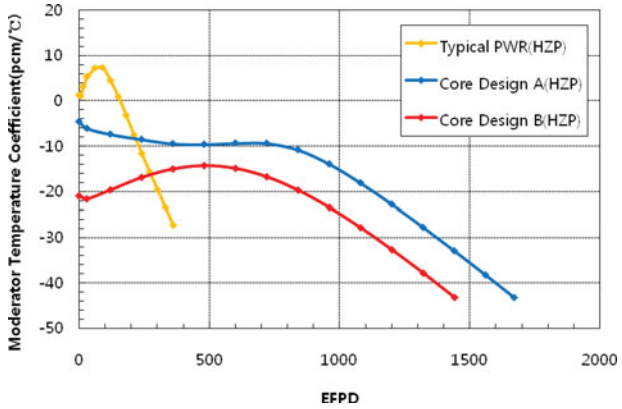


Figure 18. Comparison of MTCs (at hot zero power) for Core Designs A and B.

an example of typical commercial PWRs. These figures show that the new cores have all negative MTC values over cycle. As in Section 3.2.1, it is noted that our new cores have strong negative MTCs at EOC under HFP condition. The FTC values as a function of power rating at BOC, MOC, and EOC are compared in **Figure 20** and it shows that new cores have all negative FTC values for all power levels.

Next, the shutdown margins of the control rods are analyzed. **Figure 21** shows positions of the controls

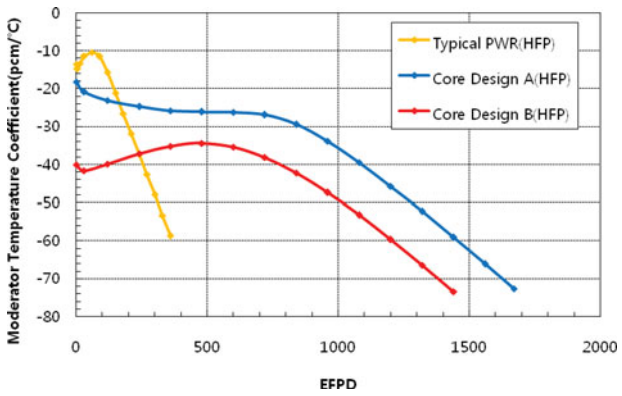


Figure 19. Comparison of MTCs (at hot full power) for Core Designs A and B.

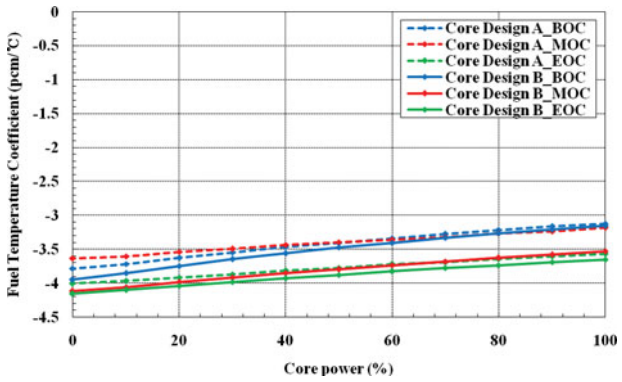


Figure 20. Comparison of FTCs for Core Designs A and B.

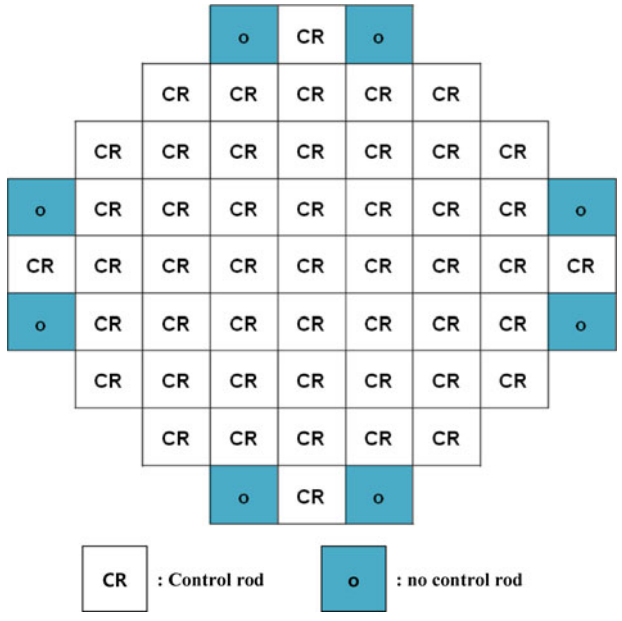


Figure 21. Positions of the control rods in the designed cores.

in the core. The absorber material of control rods is assumed to be B_4C in this work. In the present study, the detailed designs of control rods are not considered but we assumed the four finger full strength control rods used in the Korean Standard Nuclear Power Plant.

Table 4. Shutdown margin (*pcm*) for Core Designs A and B.

	Core Design A		Core Design B	
	BOC	EOC	BOC	EOC
Control rod requirement				
Power defect	1173	1907	1579	1991
Rod insertion allowance[a]				
HFP	77	112	77	112
HZP	1326	1671	1326	1671
Total requirement				
HFP	1250	2019	1656	2103
HZP	1326	1671	1326	1671
Control red scram worth				
ARI, $N-1$ (Largest control rod worth)	10,015	12,988	10,379	13,076
Uncertainty (10%)	1002	1299	1038	1308
Applied value	9014	11,689	9341	11,768
Shutdown margin				
Calculated value	7688	9670	7685	9665
Required margin[a]	6500			

Note: [a]Values from typical PWR.

The shutdown margins are summarized in **Table 4**. In calculating the shutdown margin, the rod worth requirements related with rod insertion allowances was taken from the values of typical PWRs because the rod insertion limits have not been set yet in our cores. Also, the required shutdown margins are also from the typical PWRs. Table 4 shows that our new cores have sufficient shutdown margin both at BOC and EOC.

Finally, the detailed inventories of the actinides are analyzed and the results are summarized in **Table 5**. This table shows that Core Design A has TRU destruction rate of 34.5% in FCM pins and net destruction rate of 25.4% over the core, while Core Design B has TRU destruction rate of 33.4% in FCM pins and net TRU destruction rate of 24.1% over the core. For both cores, the masses of two major plutonium isotopes ^{239}Pu and ^{240}Pu are decreased but those of the other plutonium isotopes are increased from BOC to EOC. Also, it is noted that the significant masses of ^{237}Np and ^{241}Am are significantly decreased, while those of the other

Table 5. Comparison of major actinides mass inventories (*kg*) for Core Designs A and B.

	Mass (kg, BOC/EOC)					
	UO_2–ThO_2 pin		FCM pin		Difference between BOC and EOC	
Nuclides	Core Design A	Core Design B	Core Design A	Core Design B	Core Design A	Core Design B
Th-232	3679.0/3576.6	3764.3/3665.1	0.0/0.0	0.0/0.0	[a]−102.4([b]−2.8%)	[a]−99.2([b]−2.6%)
U-233	0.0/58.4	0.0/56.8	0.0/0.0	0.0/0.0	58.4	56.8
U-235	519.0/251.8	467.2/229.9	0.0/0.1	0.0/0.1	−267.1(−51.5%)	−237.2(−50.8%)
U-238	3170.6/3063.1	2658.5/2567.0	2.1/1.6	1.7/1.3	−108.5(−3.4%)	−90.2(−3.4%)
Pu-238	0.0/1.2	0.0/0.9	18.0/39.5	14.8/31.6	22.6(+125.4%)	17.7(+119.3%)
Pu-239	0.0/35.8	0.0/30.3	319.2/90.7	262.1/79.9	−192.9(−60.4%)	−152.0(−58.0%)
Pu-240	0.0/8.7	0.0/7.2	150.8/129.6	123.8/106.9	−12.5(−8.3%)	−9.8(−7.9%)
Pu-241	0.0/7.0	0.0/5.8	45.5/58.3	37.3/48.2	19.7(+43.7%)	16.7(+44.6%)
Pu-242	0.0/1.5	0.0/1.2	33.0/43.4	27.1/35.5	11.8(+35.9%)	9.5(+35.1%)
Np-237	0.0/4.4	0.0/3.7	43.6/24.9	35.8/21.2	−14.3(−32.8%)	−10.9(−30.6%)
Np-239	0.0/0.2	0.0/0.2	0.0/0.0	0.0/0.0	0.2	0.2
Am-241	0.0/0.4	0.0/0.3	30.5/16.4	25.1/13.6	−13.8(−45.1%)	−11.2(−44.5%)
Am-242	0.0/0.0	0.0/0.0	0.0/0.0	0.0/0.01	0.0	0.0
Am-243	0.0/0.3	0.0/0.2	9.7/13.4	7.9/11.0	4.0(+41.7%)	3.3(+41.2%)
Cm-242	0.0/0.1	0.0/0.0	0.0/2.5	0.00/2.1	2.5	2.1
Cm-244	0.0/0.1	0.0/0.1	3.3/9.7	2.7/7.8	6.5(+200.4%)	5.2(+193.9%)
TRU	0.0/59.6	0.0/49.8	653.6/428.3	536.7/357.6	−166.0(−25.4%)	−129.2(−24.1%)

Notes: [a]Mass at EOC − mass at BOC.
[b](mass at BOC − mass at EOC)/mass at BOC × 100.

Table 6. Summary of core performances for Core Designs A and B.

	Core Design A	Core Design B
Cycle length (EFPD/EFPY)	1670/4.57	1440/3.95
Burnup (MWD/kgHM)	65.0	59.3
Max. CBC (ppm)	2441	1328
Power peaking factor		
Max. F_r	1.37	1.36
Max. F_q	1.68	1.77
MTC (Max./Min., pcm/°C)	−4.7/−43.3 (at HZP) −18.2/−72.7 (at HFP)	−14.3/ −43.2 (at HZP) −34.4/ −73.5 (at HFP)
TRU destruction rate (%)		
in FCM pins	34.5	33.4
in core	25.4	24.1
Shutdown margin (BOC/EOC)	7688/9670	7685/9665

minor actinides are increased. The consumption rates of ^{232}Th are about 2.8% and 2.6% for Core Designs A and B, respectively. The masses of ^{233}U at EOC for Core Designs A and B are 58.4 and 56.8 kg, respectively, that are higher than those of ^{239}Pu in UO_2–ThO_2 pins at EOC.

The main core performance parameters for these two cores are summarized in **Table 6**. These cores have 4.58 and 3.95 EFPYs cycle lengths, 65.0 and 59.3 MWD/kg average discharge burnups, respectively. As mentioned above, Core Design B has much lower initial CBC of 1328 ppm than Core Design A. Both cores have reasonable values of core performance parameters such as lower power peaking factors, negative MTCs, and sufficient shutdown margins except for high negative MTC values at EOC under HFP, which should be certified by through a safety analysis.

4. Summary and conclusions

In this paper, new small PWR cores having long cycle length of 3.95–4.6 EFPYs to significantly burn PWR-spent fuel TRUs are designed and analyzed from the view point of core neutronics. The new small PWR cores employ new fuel assembly design concepts which use UO_2–ThO_2 fuel pins and FCM fuel pins. The significant deep-burning of TRU was achieved by using the high irradiation performance FCM fuels where TRISO particles containing TRUs in their central kernels are randomly distributed in SiC matrix. Also, advanced concepts of burnable absorbers are used to reduce the initial excess reactivity of the long cycle cores and to control power peaking. The advanced concepts of burnable absorbers include BISO particles having Gd_2O_3, Er_2O_3, and B_4C kernels. Also, an IFBA-like concept of burnable absorber using ZrB_2 thin coating on pellets of UO_2–ThO_2 fuel was employed to further reduce the excess reactivity. Fuel assembly calculations showed that the addition of 50 wt% ThO_2 is a good choice in terms of the long cycle length with a fixed initial excess reactivity, and this mitigates the strong negative MTC at EOC. One of the important parts of this work is on the comparative analysis of the cores having several different reflector materials. The comparative analysis showed that the solid reflector such as graphite, SS303, and beryllium give significant extension of cycle length of the small PWR cores in comparison with the reference water reflector. In particular, it is shown that the cores using beryllium and graphite reflectors have much longer cycle length by ∼500 EFPD than the reference water reflector core and that the cores having SS303 has also longer cycle length by ∼200 EFPDs than the reference water reflector core. However, the core having beryllium reflector in spite of its longest cycle length showed high peaking factors. From this study on the reflector, the $10^w/_o$ SS and $90^w/_o$ graphite was selected as the final candidate of the reflector in order to achieve long cycle length without significantly large power peaking. With this final candidate reflector, two cores are designed and their detailed core performances including safety-related parameters are analyzed. In particular, the second design option was devised in order to reduce CBC (i.e., excess reactivity) and to simplify the core loading pattern of the first design core option.

From the detailed analysis of these cores, it can be summarized that (1) these new small PWR cores using advanced fuel assembly concept and solid reflector have long cycle length of 3.95–4.5 EFPYs and acceptable core performance parameters such as negative reactivity coefficient, sufficient shutdown margin, and low power peaking factors with one exception of too large negative MTC at EOC under HFP condition, (2) the first core design has longer cycle length but high CBC than the second design core, (3) the second core design has shorter cycle length but much lower CBC than the first one, and (4) these cores have significant TRU destruction rates of 34.5% and 33.4% in FCM pins and the net TRU destruction rates of 25.4% and 24.1% over the cores, respectively. From the study performed in this work, it can be concluded that it is possible to design long-cycle small PWR cores using advanced fuel assembly designs with FCM fuels, UO_2–ThO_2 fuels, and advanced burnable absorber concepts so as to achieve significant TRU destruction rates without degradation of core performance parameters including safety-related ones.

Acknowledgements

This work was supported by Kyung Hee University in 2012 [grant number KHU-20121703].

References

[1] Salvatores M. Transmutation: issues, innovative options and perspectives. Prog Nucl Energy. 2002;40:375–402.
[2] Yang WS. Fast reactor physics and computational methods. Nucl Eng Technol. 2012;44:177–198.
[3] Hong SG, Kim SJ, Kim YI. Annular fast reactor cores with low sodium void worth for TRU burning. Nucl Technol. 2008;162:1–25.
[4] You WS, Hong SG. A neutronic study on advanced sodium cooled fast reactor cores with thorium blankets for effective burning of transuranic nuclides. Nucl Eng Des. 2014;278:274–286.
[5] Stillman JA. Homogeneous recycling strategies in LWRs for plutonium, neptunium, and Americium management. Chicago (USA): Argonne National Laboratory; 2004 (ANL-AFCI-124).
[6] Youinou G, Vasile A. Plutonium multi-recycling in standard PWRs loaded with evolutionary fuels. Nucl Sci Eng. 2005;151:25–45.
[7] Hong SG, Venneri F, Lee KH, Cho JY, Park SY, Jo CK, Kim KY. Physics characteristic evaluation of fuel assemblies using FCM (fully ceramic micro-encapsulated) fuel for the deep burn management of transuranics in LWRs. Trans Am Nucl Soc. 2011;105:777.
[8] Hong SG, Park SY, Lee KH, Cho JY, Jo CK, Lee WJ, Venneri F. Physics study of deep-burning of spent fuel transuranics using commercial LWR cores. Nucl Eng Des. 2013;259:79–86.
[9] Venneri F, Kim Y, Snead LL, Terrani KA, Ougouag A, Tulenko JE, Forsberg CW, Peterson PF, Lahoda EJ. Fully ceramic micro-encapsulated fuels: a transformational technology for present and next generation reactors – preliminary analysis of FCM fuel reaction operation. Trans Am Nucl Soc. 2011;104:671.
[10] Snead LL, Terrani KA, Venneri F, Kim Y, Tulenko JE, Forsberg CW, Peterson PF, Lahoda EJ. Fully ceramic micro-encapsulated fuels: a transformational technology for present and next generation reactors – properties and fabrication of FCM fuel. Trans Am Nucl Soc. 2011;104:668.
[11] Cho JY, Lee JC, Lee KH, Park SY, Park HJ, Kim HY, Kim KY, Jung HJ, Song JS, Zee SG, Jo CK, Lee HC. DeCART2D v1.0 user's manual. South Korea: Korea Atomic Energy Research Institute; 2013. (KAERI/TR-5116/2013).
[12] Hong SG, Kim DY, Hyun HL, Bae GH, Park HJ. Benchmarking of depletion calculations for LWR fuel assemblies using ThO_2-UO_2 pins and TRU FCM pins. Trans Am Nucl Soc. 2013;109:1494–1496.
[13] Shim HJ, Kim CH. User's manual of McCARD version 1.1 (Monte Carlo code for advanced reactor design and analysis). South Korea: Seoul National University; 2011.
[14] Cho BO, Joo HG, Cho JY, Song JS, Zee SQ. MASTER 3.0 user's manual. South Korea: Korea Atomic Energy Research Institute; 2004, KAERI/UM-8/2004.
[15] Bae G, Hong SG, Park HJ. LWR fuel assembly designs for the transmutation of LWR spent fuel TRU with FCM and UO_2-ThO_2 fuels. Paper presented at: International Conference on Mathematics and Computational Methods Applied to Nuclear Science & Engineering (M&C 2013); 2013 May 5–9; Sun Valley, ID.
[16] Bae GH, Hong SG. Effects of the burnable poison particles in LWR fuel assemblies using ThO_2-UO_2 pins and TRU FCM pins. Trans Am Nucl Soc. 2013;109:1497–1499.
[17] IAEA. Thorium fuel cycle – potential benefits and challenges. IAEA; 2005. (IAEA-TECDOC-1450).
[18] Cho JY, Song JS, Lee CC, Zee SQ, Chang MH. 5-year cycle SMART core design using thorium fuel. South Korea: Korea Atomic Energy Research Institute; 2001. (KAERI/TR-1775/2001).
[19] Bae G, Hong SG. Neutronic design study of new small LWR core having ThO_2-UO_2 and FCM particle fuel for TRU burning. Trans Am Nucl Soc. 2014;111:272–276.